Journal of Hydrology 519 (2014) 1997–2011

Contents lists available at ScienceDirect

Journal of Hydrology

journal homepage: www.elsevier.com/locate/jhydrol

Multi-scale streambed topographic and discharge effects on hyporheic exchange at the stream network scale in confined streams

Alessandra Marzadri [a], Daniele Tonina [b,*], James A. McKean [c], Matthew G. Tiedemann [b,d], Rohan M. Benjankar [b]

[a] University of Trento, Department of Civil, Environmental and Mechanical Engineering, Via Mesiano 77, Trento 38123, Italy
[b] Center for Ecohydraulics Research, University of Idaho, 322 E. Front Street, Suite 340, Boise, ID 83702, USA
[c] Rocky Mountain Research Station, US Forest Service 322 E. Front Street, Suite 401, Boise, ID 83702, USA
[d] R2, Resource Consultants, 15250 NE 95th Street, Redmond, WA 98052, USA

ARTICLE INFO

Article history:
Received 6 June 2014
Received in revised form 24 September 2014
Accepted 27 September 2014
Available online 7 October 2014
This manuscript was handled by Corrado Corradini, Editor-in-Chief, with the assistance of Gokmen Tayfur, Associate Editor

Keywords:
Hyporheic exchange
Wavelet analysis
Streambed morphology
Confined streams

SUMMARY

The hyporheic zone is the volume of the streambed sediment mostly saturated with stream water. It is the transitional zone between stream and shallow-ground waters and an important ecotone for benthic species, including macro-invertebrates, microorganisms, and some fish species that dwell in the hyporheic zone for parts of their lives. Most hyporheic analyses are limited in scope, performed at the reach scale with hyporheic exchange mainly driven by one mechanism, such as interaction between flow and ripples or dunes. This research investigates hyporheic flow induced by the interaction of flow and streambed topography at the valley-scale under different discharges. We apply a pumping based hyporheic model along a 37 km long reach of the Deadwood River for different flow releases from Deadwood Reservoir and at different discharges of its tributaries. We account for dynamic head variations, induced by interactions of small-scale topography and flow, and piezometric head variations, caused by reach-scale bathymetry–flow interactions. We model the dynamic head variations as those caused by dune-like bedforms and piezometric heads with the water surface elevation predicted with a 1-dimensional, 1D, hydraulic model supported by close-spaced cross-sections extracted every channel width from high-resolution bathymetry. Superposition of these two energy-head components provides the boundary condition at the water–sediment interface for the hyporheic model. Our results show that small- and large-scale streambed features induce fluxes of comparable magnitude but the former and the latter dominate fluxes with short and long residence times, respectively. In our setting, stream discharge and alluvium thickness have limited effects on hyporheic processes including the thermal regime of the hyporheic zone. Bed topography is a strong predictor of hyporheic exchange and the 1D wavelet is a convenient way to describe the bed topography quantitatively. Thus wavelet power could be a good index for hyporheic potential, with areas of high and low wavelet power coinciding with high and low hyporheic fluxes, respectively.

1. Introduction

Stream waters downwell into the streambed sediment and then reemerge into the stream after some residence time within the sediment (Vaux, 1962, 1968). These fluxes stem from spatial and temporal variations of near-bed energy heads, sediment hydraulic conductivity, alluvial area, turbulence, sediment transport and the density gradient between stream and pore waters (Boano et al., 2009, 2014; Tonina and Buffington, 2009a). They create hyporheic flow, which is the main mechanism that brings oxygen-rich and solute-laden surface water into the streambed sediment (Elliott and Brooks, 1997a,b; Tonina and Buffington, 2009a; Tonina et al., 2011). Hyporheic flows also bring low-oxygen concentration reduced-element laden pore waters back to the stream from the streambed sediment (Marzadri et al., 2011, 2012b; Zarnetske et al., 2011). Hyporheic residence time and fluxes influence water quality in the sediment interstices (Boano et al., 2010; Marzadri et al., 2011; Zarnetske et al., 2012). They affect the distribution of aerobic and anaerobic conditions within the streambed, because hyporheic exchange controls the amount of surface water mixed with the pore water and the available reaction time within the sediment (Harvey et al., 2013; Marzadri et al., 2011; Tonina et al.,

* Corresponding author. Fax: +1 2083324425.
E-mail address: dtonina@uidaho.edu (D. Tonina).

http://dx.doi.org/10.1016/j.jhydrol.2014.09.076

2011; Zarnetske et al., 2011). Residence time distribution has also a strong influence on the thermal regime of the hyporheic zone (Marzadri et al., 2013a,b; Sawyer et al., 2012). Temperature is one of the most important water quality indices because of its influence on aquatic biogeochemical processes, such as those involving dissolved oxygen, nutrient and contaminants, aquatic organism metabolism, plant photosynthesis rate and timing, and the timing of fish migration (Allan, 1995; Bjornn and Reiser, 1991; Goode et al., 2013; Jonsson et al., 2004). Because of the chemical and physical gradients generated by hyporheic exchange, the hyporheic zone sustains a rich ecotone (Edwards, 1998; Stanford and Ward, 1988). Consequently, mapping hyporheic fluxes and residence time distributions is an important part of quantifying the impact of flow discharge, especially in regulated streams, on benthic and streambed environment (Kasahara et al., 2009; Kasahara and Hill, 2006a,b; Kasahara and Hill, 2007).

Hyporheic fluxes can extend vertically and laterally, depending on stream sinuosity, alluvial sediment stratification, alluvial bed thickness, bedrock outcrops and channel gradient (Bencala and Walters, 1983; Boano et al., 2007; Cardenas, 2009; Marion et al., 2008a; Stonedahl et al., 2013). They can be classified as fluvial hyporheic fluxes, which extend vertically and laterally within the channel wetted areas, parafluvial fluxes, which mainly flow below dry bars within the active channel, and floodplain fluxes, which include inter-meander fluxes and preferential flow paths along paleochannels (Buffington and Tonina, 2009; Edwards, 1998; Tonina and Buffington, 2009a).

In gravel bed rivers, the main mechanism driving hyporheic exchange is the presence of near-bed pressure gradients (Gooseff et al., 2006, 2007; Marzadri et al., 2013a; Tonina and Buffington, 2007, 2011). Its distribution depends on the interaction between surface flow and streambed topography (Elliott and Brooks, 1997a,b) at different spatial scales (Stonedahl et al., 2010). Small-scale topography, such as dune-like bed forms, logs and boulders, causes mainly dynamic head variations, which generate high and low-pressure areas upstream and downstream of irregularities, respectively (Sawyer et al., 2011; Tonina and Buffington, 2009a). For instance, low-pressure areas are present downstream of dune crests, where flow detaches, and high-pressure zones upstream of dune crests, where flow reattaches (Cardenas and Wilson, 2007d; Gualtieri, 2012; Savant et al., 1987; Thibodeaux and Boyle, 1987; Vittal et al., 1977). Conversely, large-scale topographies, such as pool–riffle sequences, generate water surface profiles and thus spatial variations of piezometric head, which is the sum of the pressure and elevation heads (Tonina, 2012). Large bed forms are typically gradually varying features that have relatively small effects on dynamic head, at least at high and moderate flows (Marzadri et al., 2013a; Tonina and Buffington, 2007).

Most hyporheic research has focused on hyporheic exchange induced by small bed forms, which may include ripples and dune-like features (Boano et al., 2007; Cardenas and Wilson, 2007a; Elliott and Brooks, 1997a; Marion et al., 2002; Packman et al., 2004; Salehin et al., 2004), whose scale is a fraction of channel width. Other studies have focused on large bed forms, such as pool–riffles (Marzadri et al., 2010; Tonina and Buffington, 2007, 2009b, 2011; Trauth et al., 2013), whose scale are several channel widths. Only recently, models have been proposed to superpose the effects of multiple topographic scales (Stonedahl et al., 2010, 2012, 2013; Tonina and Buffington, 2009b; Wörman et al., 2006).

Hyporheic exchange models that include effects of both large- and small-scale topographies are important, because they provide tools to study hyporheic exchange properties at the scale of the stream network (Marzadri et al., 2014; Stewart et al., 2011). Along stream segments we do not know how discharge, alluvial thickness and topographic variations affect hyporheic exchange induced by flow-topography interactions at multiple length-scales. The effect of multiple scale interaction on hyporheic exchange may be modulated by stream discharge (Cardenas and Wilson, 2007d; Elliott and Brooks, 1997a; Tonina and Buffington, 2011). This impact could be very important for hyporheic processes in streams whose flow regimes are regulated by dam operations (Bruno et al., 2009; Sawyer et al., 2009). Streambed thickness, which often changes along stream segments, may also affect hyporheic processes (Tonina and Buffington, 2011). We know the alluvial thickness effect on hyporheic hydraulics induced by one single length-scale interaction, but its effect on hyporheic exchange caused by multiple potentially conflicting mechanisms is less known. For instance, the influence of alluvial sediment thickness is negligible when it is thicker than one wavelength of the small-scale topography, e.g. dunes (Cardenas and Wilson, 2007a,d), or one channel width in case of large-scale topographies, like pool–riffles (Marzadri et al., 2010; Tonina and Buffington, 2011). However, we do not know which of the two mechanisms dominates and thus which of the two thresholds is more important. Furthermore, most hyporheic research focuses at the morphological unit (10^{-1}–10 times the channel width) and at the channel-reach scale (10–10^2 times the channel width) (Cardenas et al., 2004; Kasahara and Hill, 2007; Marion et al., 2002, 2008b; Wörman et al., 2002). At the network scale, both small- and large-scale topographies may vary spatially causing a distribution of hyporheic exchange. Wondzell (2011) suggested that topographic variations may provide an index of potential hyporheic exchange. This approach, which has not been tested, could be extremely useful in studying hyporheic exchange at the network scale because it would provide a tool to identify areas of high and low hyporheic exchange from relatively simple analyses of streambed topography.

Thus, here we investigate the spatial distribution of hyporheic exchange at the valley scale (10^3–10^4 times the channel width) along a 37 km long river segment of the Deadwood River (Central Idaho, USA) (Benjankar et al., 2013, 2014; Tiedemann, 2013; Tranmer et al., 2013) (Fig. 1). Different from previous analyses, where dynamic head variation models were adapted to account for the interaction between flow and topography at multiple scales (e.g., Stonedahl et al., 2013) and applied on synthetic streambeds (Stonedahl et al., 2010, 2012), here we account for both dynamic and piezometric heads by superimposing the contribution of the interaction of stream flow with small and large topographic features, measured in a natural stream.

The objectives of this study are: (i) to quantify the effects of flow discharge on hyporheic exchange at the valley scale, (ii) to understand the role of small and large scale topography in inducing hyporheic exchange, (iii) to investigate the longitudinal variation of hyporheic flow and its correlation with topographic variations, (iv) to analyze the effect of alluvium depth on the relative importance of hyporheic flow induced by small (dynamic head) and large (piezometric head) scale topography and (v) to study the effect of hyporheic flows on hyporheic thermal regime.

To reach our goals we use a hyporheic hydraulic model that couples dynamic and piezometric heads. The dynamic head is modeled as velocity head losses due to flow separation at dune-like bed forms (Elliott and Brooks, 1997b; Stonedahl et al., 2010, 2012; Vittal et al., 1977), whose amplitude and wavelength is derived from wavelet analysis of the small-scale topography along the streambed centerline. The piezometric head is quantified from the stream water surface elevations (Gooseff et al., 2006; Lautz and Siegel, 2006; Marzadri et al., 2010; Tonina and Buffington, 2007, 2011; Vaux, 1968; Zarnetske et al., 2008). Stream flow properties, including water depth, velocity and water surface elevations are predicted with a 1-dimensional, 1D, hydraulic model supported by close-spaced cross-sections, 1 channel width apart, extracted from a high-resolution digital elevation model (DEM) of the stream

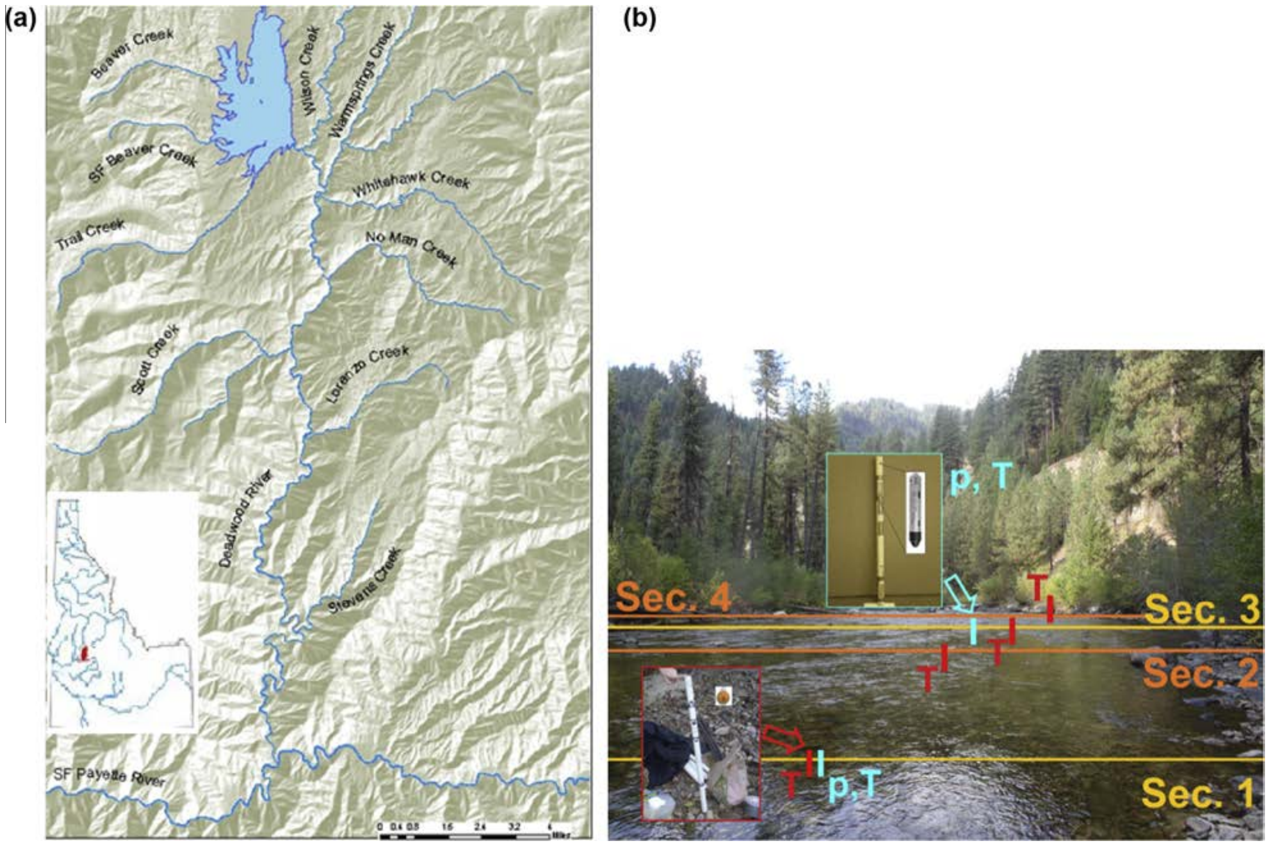

Fig. 1. (a) Deadwood River, Central Idaho, USA, between Deadwood Reservoir and the South Fork Payette River with its 7 major tributaries: Wilson Creek, Warmsprings Creek, Whitehawk Creek, No Man Creek, Scott Creek, Lorenzo Creek and Stevens Creek modeled in the simulations. The scale bar is in miles. (b) Overview of the hyporheic instrumented site sections along the Deadwood River, the positions of temperature sensors and pressure transducers are shown with red and sky-blue lines, respectively. Inset figures show the details of the PVC pipe installation for temperature sensors and pressure transducers.

bathymetry. We apply a process based model that solves the heat transport equation along any streamline connecting downwelling and upwelling areas to analyze the effects on pore-water temperature and predict temperature distributions within the hyporheic zone (Marzadri et al., 2013a).

2. Study site

The study reach is a 37 km-long section of the Deadwood River between Deadwood Reservoir and the confluence with the South Fork Payette River (Idaho, USA) (Fig. 1). Deadwood Dam was constructed for irrigation purposes in the 1930s and it regulates the stream discharge, which is augmented by 7 large and several small tributaries (Fig. 1). Dam releases dominate the stream discharge during the irrigation period, which spans early June to early September, while tributary discharge dominates during spring snowmelt, April–June, and tributary contributions equal reservoir discharges in the rest of the year. We measured tributary discharge, dam releases and water surface elevation at the end of our study site during the 2009 water year (October 1, 2008 to September 30, 2009) to use as input parameters for the 1D hydraulic model.

The river has a mean channel width at high flow of 30 m and minimum and maximum flow releases of 0 and 39.64 $m^3 s^{-1}$, respectively from the reservoir. The streambed has localized deep pools, mostly forced at bends, separated by long runs with coarse large material randomly placed along the streambed. Riffle crests are typically subdued and few cascade bedforms are localized in short areas where slope is steep.

Coarse substrate dominated by cobbles and large gravel armors the streambed with fine sediment, mainly pea gravel and sand with traces of clay, filling the voids among large particles below the coarse armor layer. Fine sediment covers the streambed only in limited patches within a few kilometers downstream of the confluence with one tributary which recently experienced debris flows.

The studied portion of the Deadwood River flows in a narrow and deep canyon with the relatively impervious canyon walls limiting the river sinuosity and restricting inter-meander groundwater connectivity. The floodplains are also quite restricted with a few small exceptions near large tributaries, which may sustain a limited floodplain and parafluvial hyporheic flows (Tiedemann, 2013; Tranmer et al., 2013). Consequently, the major component of the hyporheic flux is the fluvial hyporheic flow with negligible parafluvial and floodplain hyporheic exchanges in this system. Fluvial hyporheic exchange can be driven by clusters of sediment particles that form smaller streambed irregularities, which we modeled as dune-like bedforms, and by the larger topographic features such as pool–riffle–run–pool sequences.

3. Method

3.1. Field data

The stream bathymetry was derived from bed topography data collected with the aquatic-terrestrial Experimental Advanced Airborne Research Lidar (EAARL) system in 2007 (McKean et al., 2009). The EAARL data density is approximately 0.6 points per square meter and the data have a vertical error around 15 cm (McKean et al., 2009, 2014). These point cloud data were used to generate a 1 m grid digital elevation model (DEM) of the stream with a 10–20 cm vertical resolution. This is extensive high-resolution data set, allows a unique opportunity to study hyporheic exchange over a long stream segment (Tonina and Jorde, 2013). The DEM was used to extract cross-sections every 30 m, approximately every channel width, for a 1D hydraulic model of stream flow and to characterize the wavelengths and amplitudes of the small-scale topography.

We used a 1D wavelet analysis applied along the stream centerline of the 1 m grid to quantify the amplitude and wavelength of the streambed small-scale topography for the hyporheic model (Fig. 2) (McKean et al., 2009). We selected a 3 m-scale 2nd derivative Gaussian reference wavelet. We used the 3 m because it was small enough to detect the micro topography formed by particle clusters on the streambed. We correlated the wavelet coefficient instead of wavelet power with micro-topography amplitude and positive coefficients correspond to convex-upward topography and negative to concave-upward. We also used the wavelet coefficient values to divide the stream in reaches with homogenous small-scale amplitude to facilitate interpretation of results. This frequency domain topographic analysis predicted 15 reaches with relatively homogeneous morphology (Fig. 2). We used these reaches to investigate the effect of stream topography on hyporheic response at different stream water discharges.

A pool–riffle–run sequence was selected near the confluence with the South Fork Payette River to measure hyporheic temperatures for comparison with model predictions. The site was chosen because it represents a typical pool–riffle–run sequence of the Deadwood system and it offers an easy access for sensor deployment, maintenance and retrieval. It was instrumented with 16 temperature sensors (Onset StowAwayTidBiT, Table 2) located at 4 different cross-sections along the centerline, 4 pressure transducer sensors (HOBO water level 13′) located in 2 different cross-sections along the centerline (Fig. 1b), and 1 pressure transducer sensor left in the open air to measure barometric pressure. Both temperature and pressure sensors were housed in PVC pipe (Fig. 1b) as done in previous field works (e.g., Gariglio et al., 2013; Tonina et al., 2014).

At each location, temperatures were recorded every 15 min by nesting four TidBiT sensors in PVC pipe (see Fig. 1b) (Table 2). The upper end of the vertical array was located at the streambed to provide data within the hyporheic sediment at 10, 20 and 50 cm below the streambed, respectively. Near to the temperature probes, two pressure transducer sensors were installed that recorded both pressure and temperature every 15 min. This was accomplished by nesting two Onset HOBO U20 Water Level Loggers in a PVC pipe (Fig. 1b) (Table 2). The topmost water level indicator was located at the streambed water interface while the other was placed within the hyporheic sediments at 50 cm below the streambed.

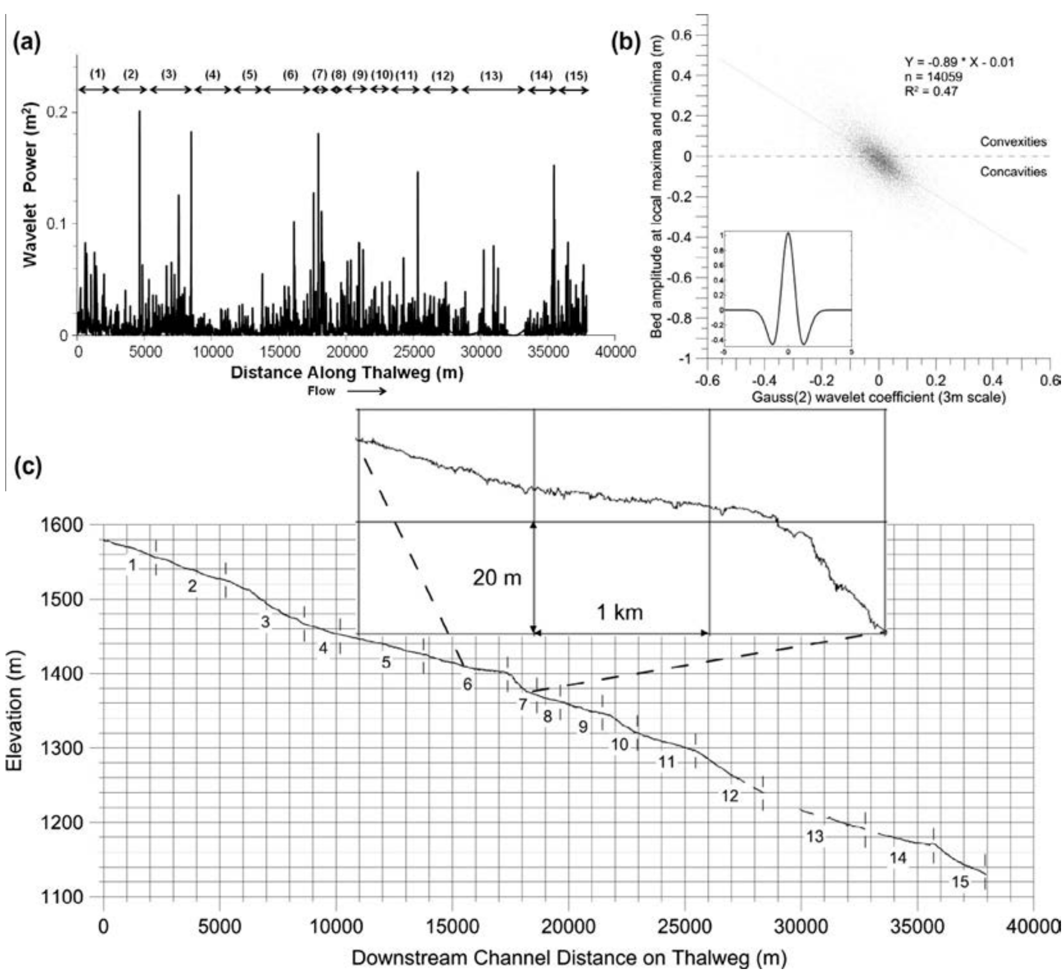

Fig. 2. Wavelet analysis of the streambed topography along the river centerline. Panel (a) shows the wavelet power for the 3 m scale wavelet along the Deadwood River and (b) the relationship between bed amplitude and wavelet coefficient. This information was used to quantify the averaged small-topography amplitude over channel lengths corresponding to about 1 channel width. Panel (c) shows the longitudinal profile of the stream.

Table 1
Discharge scenarios modeled in the analysis.

Scenario	Reservoir releases ($m^3\ s^{-1}$)	Date range
1. Winter	0	5–1–2009 → 24–2–2009
2. Winter	0.05	5–1–2009 → 24–2–2009
3. Winter	1.42	5–1–2009 → 24–2–2009
4. Spring: pre ramping	11.33	20–6–2009 → 5–7–2009
5. Spring: ramping	16.42	15–7–2009 → 20–7–2009
6. Summer: high flow	27.18	4–8–2009 → 27–8–2009

Table 2
Main characteristics of Onset HOBO pressure and temperature sensors.

Sensor type	Measurements range	Resolution	Accuracy
Oneset HOBO pressure	0–145 kPa	0.02 kPa	±0.14 kPa
Oneset HOBO temperature	−20–50 °C	0.1 °C	0.1 °C

The PVC pipes were perforated at each sensor location to allow direct contact with streambed sediments and seepage water (Gariglio et al., 2013). In order to prevent vertically preferential flow paths within the PVC pipe, disks of Styrofoam material and fine stream bed sediments were inserted in between sensors. Both pressure and temperature sensors were checked prior to and following deployment for temporal or thermal drift by testing their measurements in a temperature-controlled water bath. Data collection began on 10/02/2011 and ended on 09/28/2012 for the TidBit temperature sensors; while the Onset HOBO U20 Water Level Logger data collection began on 10/02/2011 and ended on 05/15/2012.

3.2. Surface flow modeling

Surface water hydraulics was modeled with a 1D hydraulic model (MIKE11®). Time series of measured outflows from the reservoir and discharges measured at the major tributaries were used as inflow boundary conditions and the downstream boundary was set as a discharge-stage rating curve (Tiedemann, 2013). Cross-sections were extracted from the stream DEM every 30 m, which corresponds to the averaged bankfull width, along the centerline to define the channel flow geometry. This provided an unprecedented high-resolution stream network for a 1D model and the ability to have mean flow velocity, depth and water surface elevation to drive the hyporheic models (small and large scale) every 30 m (Pasternack and Senter, 2011; Tonina and Jorde, 2013).

The inaccessibility of the stream during high flows and for most of its course even at low flows, coupled with poor reception for obtaining precise ground Global Position System (GPS) locations and elevation measurements, reduced the possibility to gather data for thorough model calibration. Thus, we selected a value of Manning's n equal to 0.06 for the entire reach (Tiedemann, 2013) based on literature review of roughness coefficients for similar types of streams (Barnes, 1967; Rosgen, 1994, 1996). Because it was not feasible to measure water surface elevation along the entire reach at different flows, we validated the selected value with two tests comparing: (a) predicted and observed water surface elevations collected at low flow conditions (1.42 $m^3\ s^{-1}$) at two 100 m long accessible reaches near the two ends of the study site and (b) predicted and observed flood wave hydrographs in a 100 m long reach near the confluence with the South Fork Payette River. The latter allowed us to check the uncertainty caused by n on the water surface elevation over a range of discharges simulated in the reach. The first test resulted in root mean square error of 20 cm between measured and predicted water. The error is large, but not unusual for 1D modeling at this large scale (Parkinson, 2003). It is comparable to the uncertainty on the measured water surface elevations due to poor GPS accuracy within the canyon. The second test showed that the model captures the timing of flood waves well moving through the system. Comparison between predicted and measured discharges have an R^2 of 0.98 and a root mean square error of 1.48 $m^3\ s^{-1}$ (Tiedemann, 2013). This last test checked the quality of the model over a range of discharges between 1.42 and 27.18 $m^3\ s^{-1}$. Manning's n values typically decrease with increasing discharge. The decrease is large at low flows and small at high flows. Because of the limited information at high flows along the stream, we were not able to rigorously test whether the Manning's n decreased with flow. However, our check based on the timing of the flood wave suggests that the chosen value is adequate for the studied range of flows.

The model was run for six discharge scenarios from base to high flows (Table 1). These scenarios are representative of the annual pattern of reservoir releases and of the flow regime of the tributaries. The 0, 0.05 and 1.42 $m^3\ s^{-1}$ are three winter flow releases from the reservoir. The 0 discharge means that only tributaries are effectively providing flow. The 11.33 and 16.42 are spring flow releases and the 27.18 is the summer flow release from the reservoir. Discharge increases downstream as tributaries enter the main stem of the Deadwood River and their contributions vary during the year.

3.3. Hyporheic flow modeling

The entire study site is located in a narrow canyon with limited depositional material and bedrock walls shaping the plan form of the stream (Fig. 1). Consequently, the system can be schematized with non-erodible banks, without any hyporheic exchange between meanders and a thin alluvium layer. We accounted for both small and large topographical variations by superposing the effects of small and large topographic features (Fig. 3). We used a two-dimensional, 2D, hyporheic model developed from those proposed by Stonedahl et al. (2010), Elliott and Brooks (1997a, 1997b) and Tonina and Buffington (2007, 2011) (Appendix A.1). Stonedahl et al. (2013) adopted Elliott and Brooks dune-generated near-bed pressure distribution for both small and large bedforms. For the latter, they used the bar amplitude and wavelength to approximate the head profile induced by the large-scale topography; effectively they associated the hyporheic exchange induced by the interaction between flow and large-scale topography with dynamic instead of piezometric heads. Here, we used the water surface elevation predicted with a 1D hydraulic model to defined the piezometric head gradient due to the interaction between stream flow and large-scale topography (Gooseff et al., 2006; Vaux, 1968; Zarnetske et al., 2008). We studied the effect of each head gradient separately to understand the relative importance of each mechanism and then combined the two scales of processes.

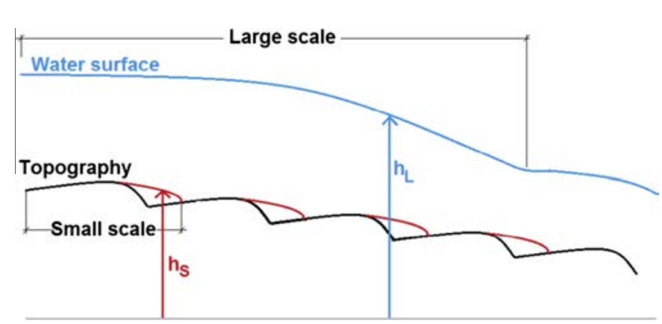

Fig. 3. Sketch showing the effects of small, h_s, and large, h_L scale topography on near-bed pressure heads $h_T = h_s + h_L$.

Groundwater basal flow, longitudinal flow chiefly induced by valley slope, which modulates the hyporheic flow vertical extension (Cardenas and Wilson, 2007c; Marzadri et al., 2010), was modeled as the product between sediment hydraulic conductivity and reach mean streambed slope. We neglected the interaction between stream and ambient groundwater, the vertical groundwater flow responsible for gaining or losing conditions (Fox et al., 2014; Hester et al., 2013), by assuming no net discharge between these two systems, which is reasonable due to the thin alluvial depth.

The developed model was coupled with a temperature model, which accounts for conduction, advection and longitudinal diffusion (Marzadri et al., 2013a) (Appendix A.2). The details of both model developments are reported in the Appendix section. The hyporheic hydraulic model assumes constant and isotropic hydraulic conductivity, which was selected equal to 0.005 m s^{-1}. This value was verified by comparing model simulated and measured hyporheic temperatures. We set the impervious layer at 1, 5 and 30 m below the streambed surface to investigate the influence of alluvium thickness on the relative importance of dynamic (small topography) and piezometric (large topography) heads.

Residence time and hyporheic flux were quantified with a particle tracking technique (e.g., Tonina and Bellin, 2007). Particles were spaced 2 cm apart along the longitudinal direction and released at the water sediment interface. We tracked and counted only those particles that re-entered the stream after flowing within the streambed sediment for calculating flux and median residence time. These last two values were quantified by averaging the hyporheic fluxes and calculating the median of the residence times over a 300 m section to set the average local mean hyporheic flux. Flux and residence times were then calculated over each reach to quantify the global exchange at the reach scale. We selected a 300 m section for our local exchange because most large topographic features such as pool–riffle extend over several channel widths, which may range between 5 and 10 (Leopold and Wolman, 1957; Montgomery and Buffington, 1998). Thus, a section of 10 channel widths should provide a representative section of stream with enough topographic variation.

In order to quantify the role of the hyporheic zone on in-stream water temperature, the following parameter Δ_{amp} was introduced to represent the ratio between the mean amplitude of upwelling temperature over 30 m ($T_{A,30}$) and the amplitude of the in-stream water temperature (T_A) (Sawyer et al., 2012):

$$\Delta_{amp}(x) = \frac{T_{A,30}}{T_A} \tag{1}$$

Values of Δ_{amp} close to 0 represents zones where the mean amplitude of upwelling temperature is much lower than the amplitude of the in-stream water temperature. We then averaged this value over each channel reach to provide an average response of the hyporheic zone.

3.4. Hyporheic model validation

The PVC pipe with the TidBit sensors in Section 2, the uppermost TidBit in Section 3 and the TidBits at −20 and −50 cm in Section 4 were found at the end of the irrigation season (Fig. 1b), the others were lost or damaged during the field experiment. High flows probably removed or buried the probes at Sections 1 and 3. The probe at Section 4 was found with the upper part of the PVC pipe broken, which could have been caused by sediment transport. The sensors left in the stream were found buried at the time of retrieval. We assume that sediment transport deposited sediment on top of the sensors during high flows. Inspection of the flow hydrographs shows that high flows started during the end of April at the beginning of the snowmelt period. Consequently, we were not able to use the late spring data for checking model performance. Analysis of the temperature data during the fall and winter times showed limited or subdued stream water daily temperature oscillations. During the recorded period with well-defined stream water daily temperature fluctuations, we selected a 3-day period between 04/13/2012 and 04/15/2012 to compare the predicted and measured data because the hyporheic mean daily temperatures did not differ from that of the surface water and therefore it was suitable for interpretation within the temperature model (Marzadri et al., 2013a,b). We used MIKE 11 hydraulic predictions to inform the hyporheic model at the water–sediment boundary and an impervious layer at the bottom of the alluvium set at 1 m below the streambed surface elevation. The mean measured temperature at 50 cm below the sediment was used as the groundwater temperature. The thermodynamic parameters used in the simulations are reported in Table 3. According to the data reported by Niswonger et al. (2005) and considering that the streambed sediment is characterized mainly as surface cobbles with gravel and sand beneath, it was assumed that the heat capacity of the soil was $C_s = 1.6 \cdot 10^6$ J m^{-3} °C^{-1} (Table 3).

The temperatures predicted by the temperature model and those measured in the hyporheic zone of the Lower Deadwood River, were generally in good agreement (Fig. 4). Measured and modeled signals are in phase and usually have comparable maximums and minimums with the largest amplitude differences in the deepest probe in Section 4 (Fig. 4f). The small disagreements in amplitude between the modeled and the measured values are probably due to the fact that the model neglects thermal disequilibrium between solids and water, lateral diffusion and mixing with the groundwater, which may have caused the subdued sensor response at 42 cm depth in Section 4 (Marzadri et al., 2013a,b; Rau et al., 2012). The modeled timing of the maximum and minimum is generally near that of the measured value, although in some cases it is slightly earlier than the measured. Because the timing of highs and lows mostly depends on hyporheic velocity, this confirms that the selected hydraulic conductivity is adequate or slightly larger.

4. Results and discussion

4.1. Effects of small and large scale topography on hyporheic flow

We ran the hyporheic model separately with only dynamic (small-scale topography) and piezometric (large-scale topography) heads to quantify the relative importance of small (Fig. 5a and c) and large (Fig. 5b and d) scale topographic features on the median hyporheic residence time, τ_{50}, and upwelling hyporheic flux, q_{uw}, for the 6 different discharge scenarios along the 15 reaches. The reaches are arranged by progressive downstream distance from Deadwood Reservoir. The median hyporheic residence time represents the time at which 50% of the downwelled particles exited the hyporheic zone.

The reach-averaged median hyporheic residence time, τ_{50}, for the two flow-topography interactions are one order of magnitude different. Whereas the small topography induces τ_{50} on the order of a fraction of day to a day, the latter is on the order of several days. The τ_{50} of hyporheic solely induced by piezometric head variations is associated with long hyporheic flow lines, which are comparable to several channel widths (Marzadri et al., 2010; Trauth et al., 2013). Consequently, it results in longer residence times compared to those caused by the small topography. This latter topography causes hyporheic flow paths of length scale of the order of a fraction of one channel width. This finding is comparable to the analysis of Stonedahl et al. (2013), who showed that bars cause residence times longer than those of dunes in a set of synthetic river reaches. Our analysis shows that both large and small topographies have the potential to generate comparable hyporheic fluxes (c.f. Fig. 5c and d).

Table 3
Values of thermodynamic parameters used in the simulation for modeling temperature measurements along the Deadwood River, Idaho. C_w is the heat capacity of the water, C_s, the heat capacity of the sediment, C is the effective volumetric heat capacity of the sediment–water matrix ($C = \phi C_w + (1-\phi)C_s$), Ke is the average bulk thermal diffusivity, K_T is the effective thermal conductivity, ϕ is the porosity of the sediment, α_L is the longitudinal component of the dispersivity, T_0 is the mean in-stream water temperature, T_{GW} is the ground water temperature, T_A is the amplitude of the sinusoidal variation of the in-stream temperature and td is the period of the temperature oscillations.

C_w (J m^{-3} °C^{-1})	C (J m^{-3} °C^{-1})	C_s (J m^{-3} °C^{-1})	C_T (–)	K_T (W m^{-1} °C^{-1})	Ke (m^2 d^{-1})	ϕ (–)	α_L (m)	t_d (day)	T_0 (°C)	T_{GW} (°C)	T_A (°C)
$4.2 \cdot 10^6$	$2.6 \cdot 10^6$	$1.6 \cdot 10^6$	1.62	1.8	0.06	0.38	0.01	1	12	6	4

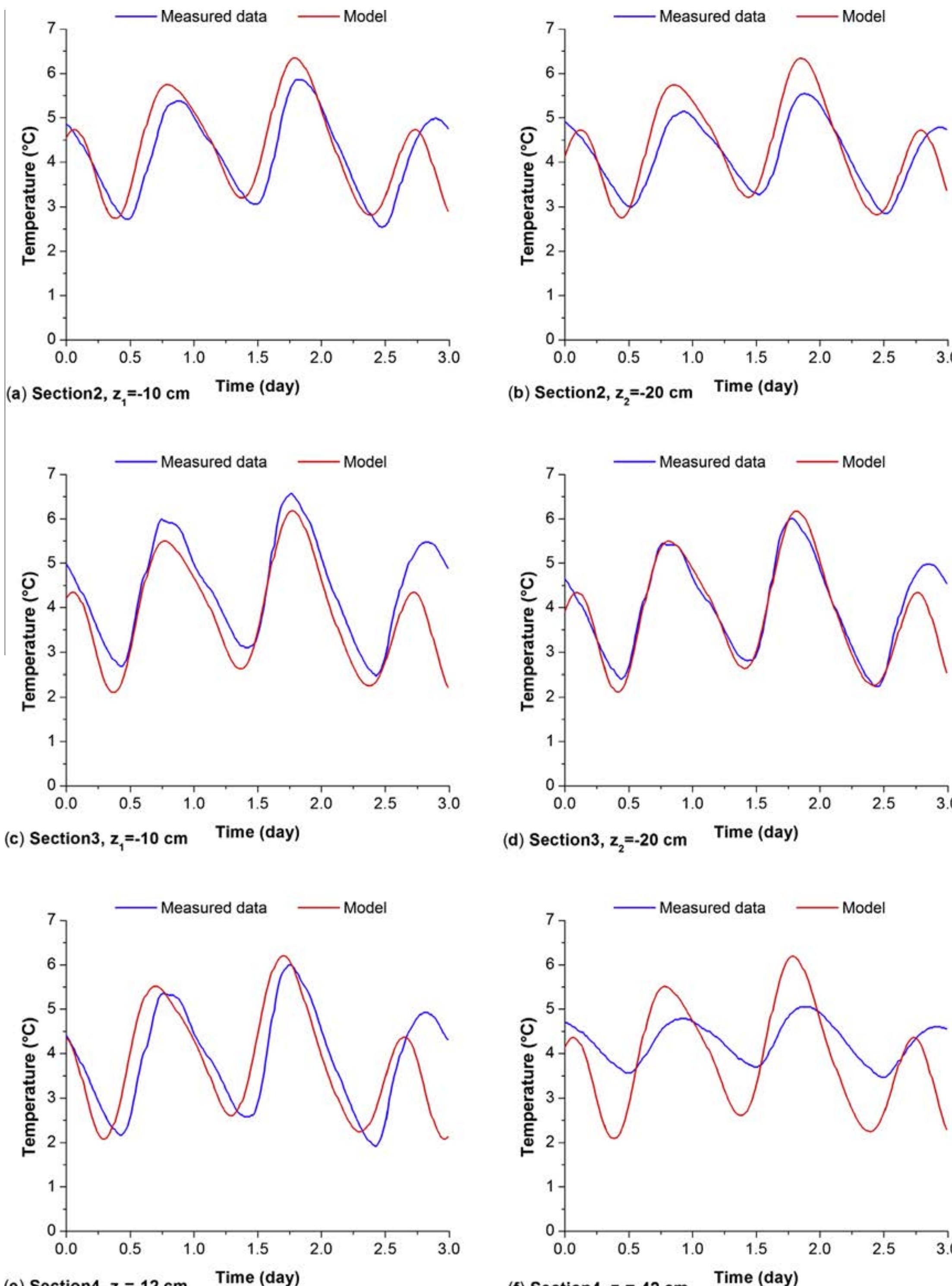

Fig. 4. Comparison between model-predicted and the field-measured temperatures in Section 2 at depths (a) $z_1 = -10$ cm and (b) $z_2 = -20$ cm, Section 3 at (c) $z_1 = -10$ cm and (d) $z_2 = -20$ cm and Section 4 at (e) $z_1 = -12$ cm and (f) $z_2 = -42$ cm.

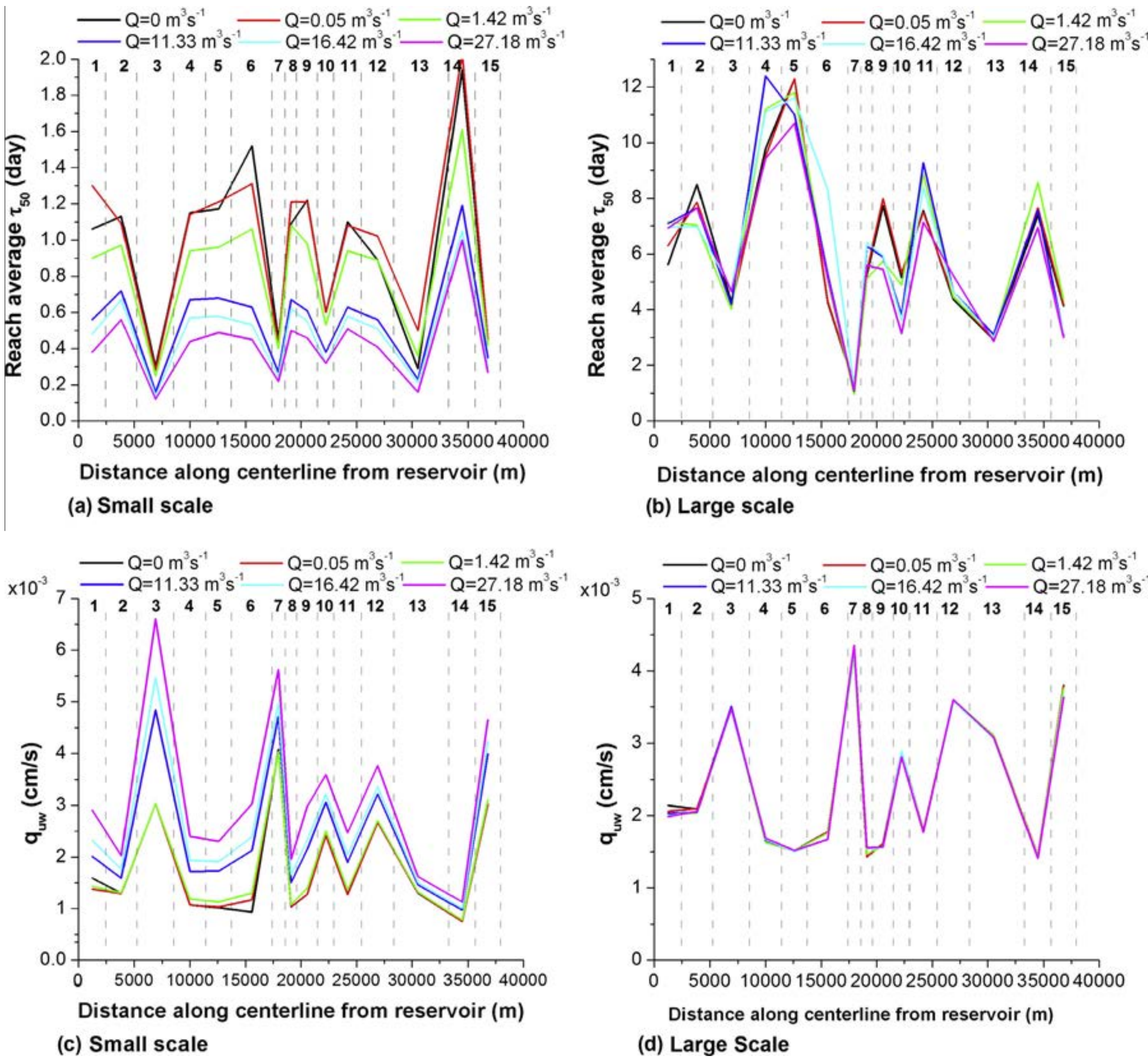

Fig. 5. Effects of discharge over small scale (left panels) and large scale topography (right panels) on median hyporheic residence time (τ_{50}) (top panels) and upwelling flux (lower panels).

These results show that the two scales of flow-topography interactions induce comparable hyporheic fluxes but with 2 different time scales in this system. The small scale interaction causes shorter residence time than the large scale interaction (Stonedahl et al., 2010; Tonina and Buffington, 2009a). The former is nested over the latter as it develops over one or few small features (less than a channel width) whereas the latter extends over one or more channel widths (Woessner, 2000). Thus, the two mechanisms may affect the type of biogeochemical transformations that occur within the streambed sediment. The hyporheic zone of the small scale topography may be potentially dominated by aerobic conditions because of the short residence times whereas that of the large-scale topography by anaerobic (Kennedy et al., 2009; Marzadri et al., 2011, 2012b; Zarnetske et al., 2011). Alternatively, high microbial activity in the streambed may create strong chemically reducing conditions in these short flow paths beneath small streambed geomorphic features (Harvey et al., 2013).

4.2. Effects of discharge on small-scale and large-scale topography interaction

As the flow discharge increases, passing from scenario 1 ($Q = 0\ m^3\ s^{-1}$) to scenario 6 ($Q = 27.18\ m^3\ s^{-1}$), the median hyporheic residence time induced by either small or large topography generally decreases. The impact is much larger in the small-scale topography (Fig. 5a, and c), more in response to the larger increase in flow velocity than flow depth in this channel with a steep streambed slope. Their combined effect is to increase the amplitude of near-bed head distribution, h_m, and thus the mechanisms driving hyporheic flow at the small scale (see Eq. (A1.3)). The dynamic-head model for small scale-topography shows that hyporheic residence time should increase with flow depth but decrease with increasing mean flow velocity (Elliott and Brooks, 1997b). Conversely, Fig. 5b shows that the τ_{50} solely due to the large-scale-topography flow interaction is less dependent on stream discharge. The negligible dependence on discharge is due to the fact that modeled water surface elevation profiles at different discharges are almost parallel to one another, which causes constant piezometric heads. Contrarily to τ_{50}, hyporheic fluxes induced by the small topography increase with stream discharge, whereas those caused by the large topography show negligible dependence with stream flow.

4.3. Effects of discharge on hyporheic flow

Fig. 6a shows the distribution of the reach-averaged upwelling hyporheic flux induced by superposing all the hyporheic mechanisms over each reach for the 6 different flow scenarios along with the averaged small-topography head amplitude (h_m). Downwelling fluxes have similar values to upwelling but with the opposite sign and therefore are not reported. For each scenario, the distribution of the reach-averaged upwelling flux changes from upstream to downstream reaching the maximum value in reach 7. This maximum value stems from the presence of the largest head amplitude for both small and large-scale topographies (Fig. 6a). This reach is the steepest and has large topographic changes (Fig. 2), which cause large hyporheic exchange at both small and large topographies.

Interestingly, the trend of the h_m, tracks very well the trend of hyporheic fluxes generated by small topography (Fig. 5c), large topography (Fig. 5d) and their combination (Fig. 6a). Consequently, the spatial trend of the total reach-averaged hyporheic flux is similar to that of the hyporheic flow induced by the large and small topography (c.f., Fig. 5c, d and Fig. 6a). However, similar to the large-topography induced hyporheic fluxes (Fig. 5), the reach-averaged flux has only a small dependence on stream discharge (Fig. 6). The smaller dependence on discharge of the total flux than the small-topography induced flux could be because the small-scale hyporheic flow is enveloped within the flow generated by the large-topography and its intensity is modulated by the large topography. Conversely, τ_{50} averaged over each reach of the Deadwood River decreases as discharge gets larger (Fig. 6b). τ_{50} varies with reach and presents its minimum value in reach 7, because of the largest fluxes in this section of the river.

4.4. Effects of alluvium thickness on reach-averaged hyporheic flow

As the thickness of the hyporheic zone increases, the reach-averaged upwelling flux remains almost constant, whereas the median hyporheic residence time undergoes some, but limited, increase with thickness. Alluvium thicknesses of 1 and 5 m, which are reasonable for this stream, cause only small differences in hyporheic exchange and a deep alluvium of 30 m is required to have visible effects on the hyporheic residence time. As observed by Zijl (1999), the flow field generated by the small scale head variations dominate the shallow depth hyporheic fluxes, whereas the deep streamlines are almost entirely governed by the large scale head variations (Fig. 7). The former are linked with the bed-form wavelength, which is 3 m in our case. Thus variations between 1 and 5 m do not affect the influence of the small scale topography. However, the vertical influence of the large scale topography is linked with the channel width. Thus the influence of the flow-large topography interaction increases as alluvial thickness approaches the channel width.

4.5. Streambed topography as an index of hyporheic flows

Fig. 8a shows the reach-averaged hyporheic upwelling flux for the two extreme flow scenarios versus the normalized wavelet power of each reach. The latter is an index of the amplitude and spatial scale of streambed topography and also head variation at the small scale. The wavelet power tracks the areas of high and low fluxes as hyporheic flux increases with wavelet power reasonably well (Fig. 8a). Similarly it tracks also the locations of high and low residence times but with an inverse relationship: areas with small wavelet power have long residence times and those with high wavelet power have short residence times. This highlights the importance of the streambed topography. Although, the wavelet power was run at the wavelength of the small bed topography, it also well represents the total (small and large topography induced) hyporheic exchange. Because wavelet power analysis does not directly depend on hydraulic modeling but only on streambed morphology, it could be used as an index of relative hyporheic potential (Boano et al., 2014; Wondzell, 2011). This approach could be quite useful to efficiently map areas of high and low potential hyporheic exchange throughout stream networks as extensive streambed bathymetry becomes more common. However, it is important to remember that hyporheic exchange is not solely determined by bed topography, but can be modulated also by the interaction with the larger groundwater system, which may inhibit or limit the exchange (Cardenas and Wilson, 2007c; Fox et al., 2014; Hester et al., 2013).

4.6. Effects of discharge on temperature regime

Fig. 9a shows the temperature attenuation (Δ_{amp}) for the two extreme discharge scenarios versus wavelet power. Discharge appears to have only a weak effect on the hyporheic temperature attenuation, similar to the observation for the hyporheic flux and residence time. Δ_{amp} also has the same trend with wavelet power, although the relationship is much weaker than for hyporheic flux. Areas of the channel with higher amplitude bed topography have greater spectral power and correspond to reaches with smaller temperature attenuations (Fig. 9a), which is consistent with their

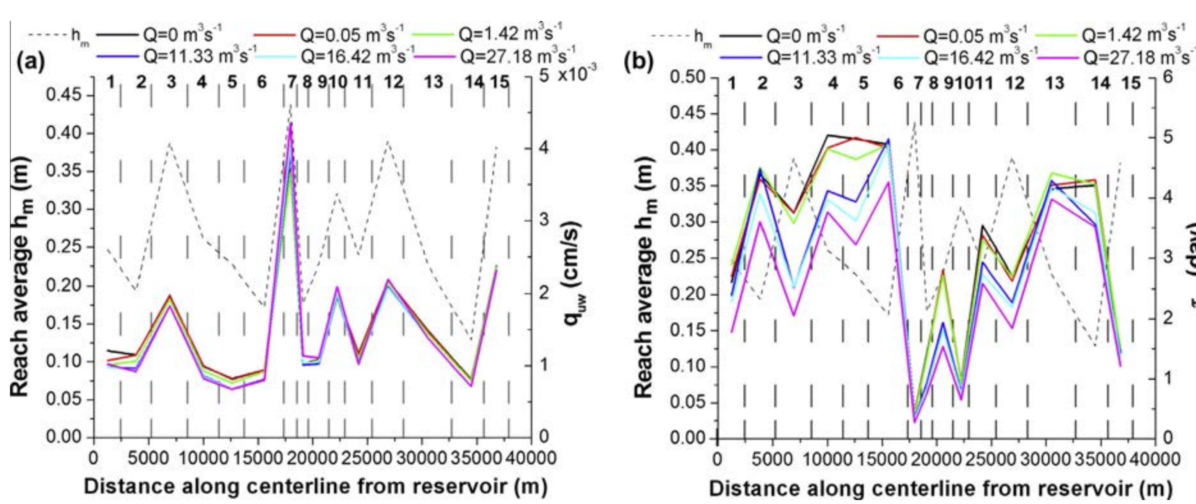

Fig. 6. Comparison between the distribution of mean hyporheic upwelling flux (q_{uw}) and the reach average dynamic head fluctuation (h_m) and the distribution of median hyporheic residence time (τ_{50}) and the reach average dynamic head fluctuation (h_m) along the Deadwood River for six discharge scenarios. The 15 reaches are arranged by progressive distance from Deadwood Reservoir.

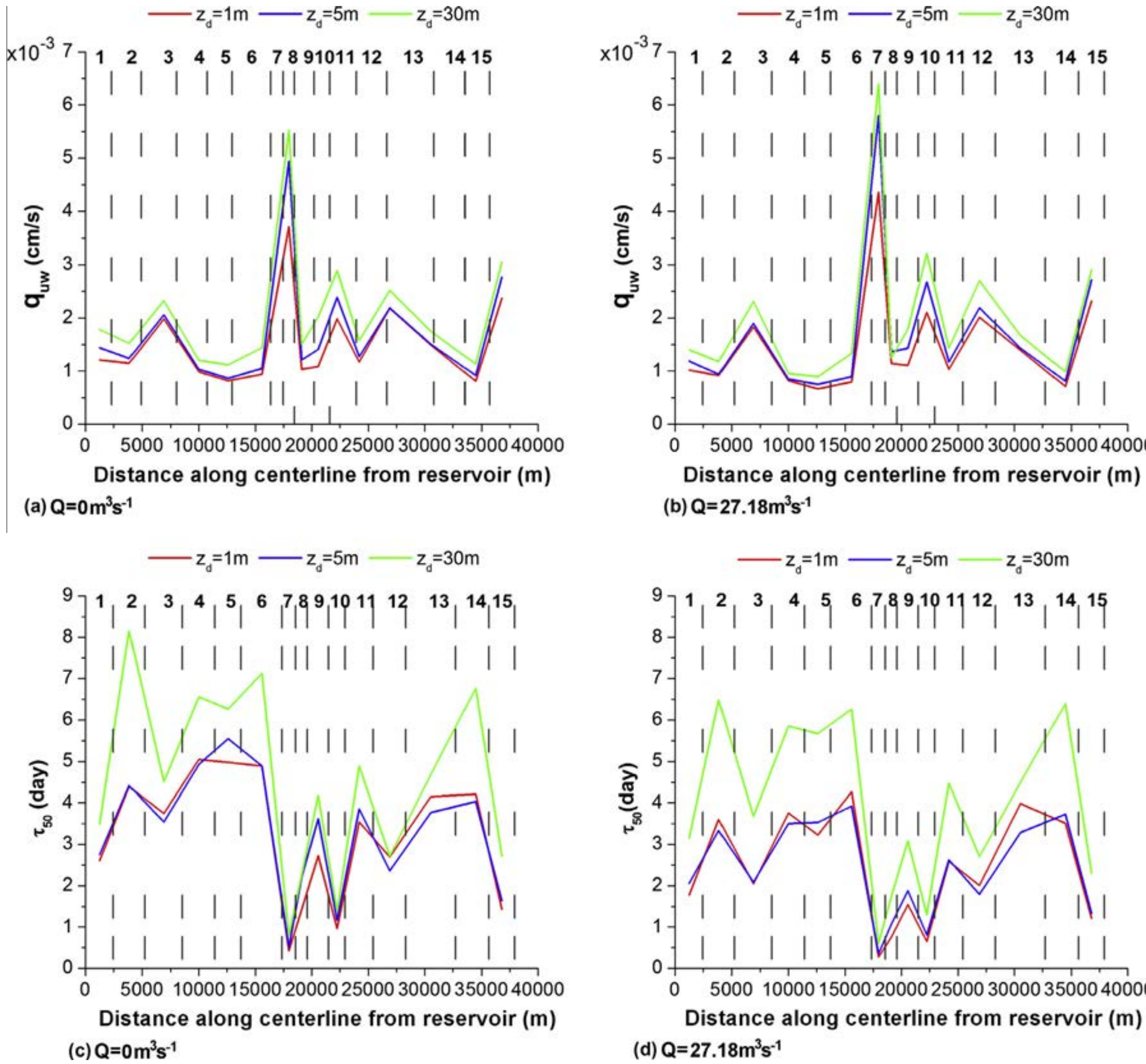

Fig. 7. Effects of alluvium thickness on the hyporheic fluxes (upwelling) (top panels) and median residence time (lower panels) for the two extreme water discharge scenarios: Scenario 1 $Q = 0\ \mathrm{m^3\ s^{-1}}$ (left panels) and Scenario 6 $Q = 27.18\ \mathrm{m^3\ s^{-1}}$ (right panels).

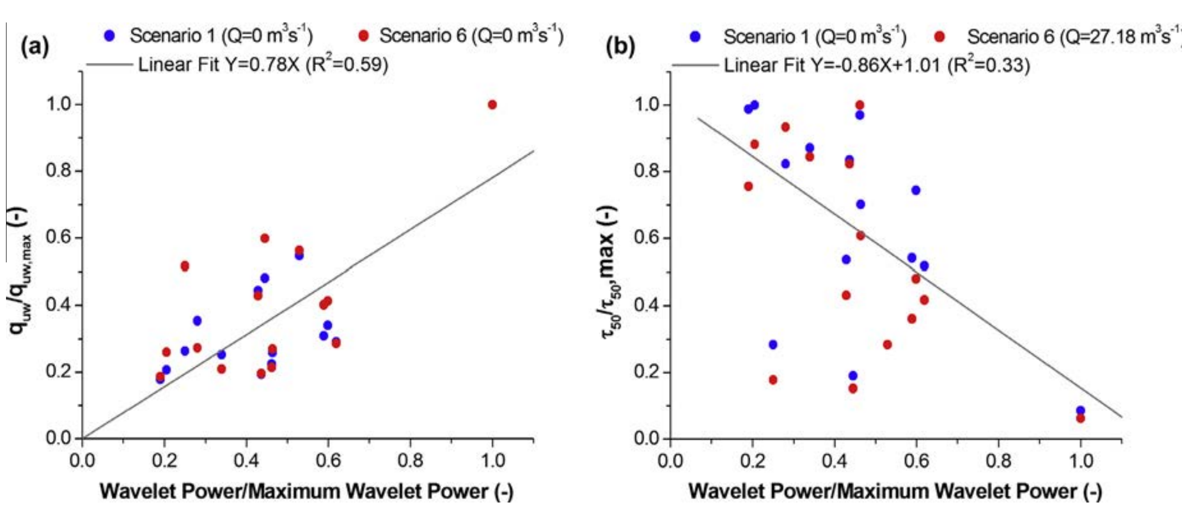

Fig. 8. Trend of variation of the normalized hyporheic (a) mean upwelling flux and (b) mean median residence time for the two extreme scenarios (Scenario 1 and Scenario 6) as a function of the normalized wavelet power.

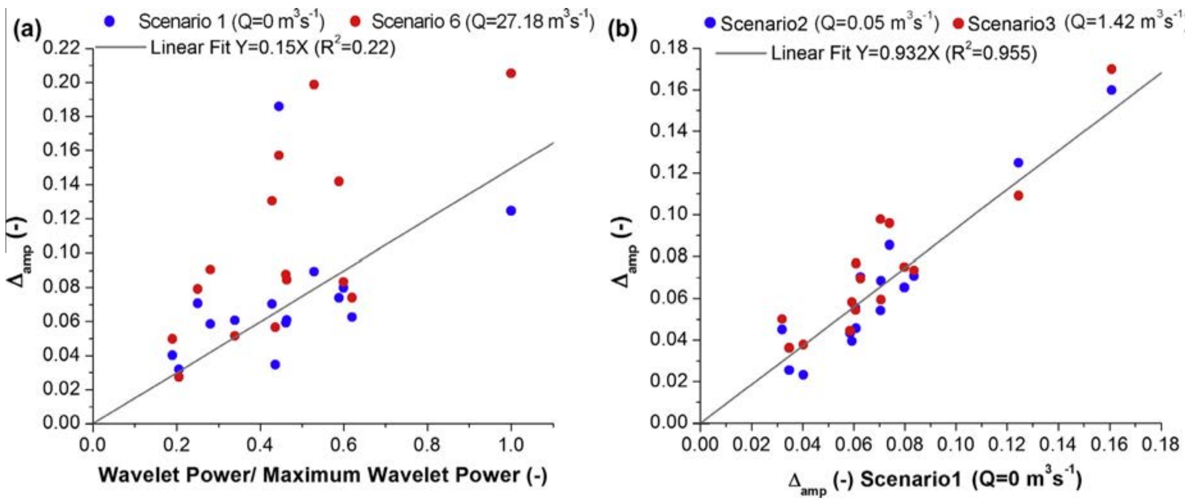

Fig. 9. (a) Trend of variation of the temperature attenuation (Δ_{amp}) as a function of the wavelet power for the two extreme scenarios: Scenario 1 ($Q = 0$ m^3 s^{-1}) and Scenario 6 ($Q = 27.18$ m^3 s^{-1}); (b) comparison of amplitude ratio between stream and hyporheic mean response for Scenario 1 $Q = 0$ m^3 s^{-1}, Scenario 2 $Q = 0.05$ m^3 s^{-1} and Scenario 3 $Q = 1.42$ m^3 s^{-1}.

longer hyporheic residence times and higher hyporheic flux (Fig. 8) Moreover, Fig. 9b shows that hyporheic hydraulics induced limited changes in the temperature attenuation during the three winter flow scenarios.

The value of Δ_{amp} is very small in this system. This suggests that daily temperature fluctuations may be less important than the daily mean temperature on hyporheic processes. Consequently, hyporheos habitat may mostly depend on daily average temperature rather than on temperature oscillation (Marzadri et al., 2013b). This result and the small dependence of hyporheic thermal response on stream discharge suggest that the hyporheic zone of this stream is thermally stable at the daily time scale.

5. Conclusion

We analyzed the hyporheic exchange induced by stream flow interaction with both small and large spatial scale topographies at multiple discharges and for multiple alluvium thicknesses along a 37 km long confined stream. We used a simplified 2D hyporheic model with homogeneous and isotropic hydraulic properties of the sediment. The model neglected ambient groundwater and any lateral flows. This last assumption is reasonable because the alluvial depth is thin and ground water most likely forms basal flow, which is accounted for in the model. The model is modified from that proposed by (Stonedahl et al., 2010) to account for both small and large scale processes. Near-bed pressure distributions were defined by superimposing the dynamic head variations induced by small topographies, whose length scale was about 3 m, and the static head profile due to the interaction between flow and large scale topography, e.g., pool–riffle bedforms. The temperature model is 2D and accounts for longitudinal, but not transversal, dispersion. It assumes thermal equilibrium between the sediment and the water. We anticipate that model performance could be somewhat improved in the future by removing this assumption.

Our results show that hyporheic exchange induced by only small-scale topography (mainly dynamic head variations) depends on stream discharge whereas that due to large-scale topography (mainly piezometric head variations) has little discharge dependence. When these spatial scales are combined in the analysis, the larger scale dominates. This result could be different in unconfined streams where parafluvial and floodplain hyporheic zones are active.

Alluvium depth is typically limited in this type of mountainous stream (0–5 m) and moderate changes of its thickness (within a few meters) have negligible effects on the hyporheic exchange. Some effects of the alluvium thickness are visible on the residence time distribution, while they have minimal impact on flux magnitude.

The thermal regime of the hyporheic flow in this system appears to be quite stable. It depends only weakly on stream discharge, that varied over several cubic meters-per-second. Likewise, variations in alluvium thickness, within the range of 1–5 m, had little effect on temperature. The primary control on the hyporheic thermal regime appears to be the daily mean stream water temperature. Thus hyporheos and other streambed sediment dwelling organisms are able to live in a very stable temperature environment.

Bed topography is a good predictor of hyporheic exchange and the 1D wavelet is a convenient way to quantitatively describe the bed topography. Thus, wavelet power could be a good index for hyporheic potential of streams.

Acknowledgments

We thank Dr. S. Stonedahl and Dr. J.W. Harvey for their constructive criticism and comments. This research was partially supported the United States Forest Service Grant 08-JV-11221659-036. Additional funding was provided by Center for Ecohydraulics Research (CER) and University of Idaho (UI) Research Office. We would like to thank the DHI (Danish Hydraulic Institute) for providing MIKE software packages to the University of Idaho. Any opinions, conclusions, or recommendations expressed in this material are solely those of the authors and do not necessarily reflect the views of the supporting Institutions and Agency.

Appendix A:. Hyporheic model

A.1. Hyporheic flow modeling

We assumed impermeable river banks in this confined mountain river with limited alluvial depth, z_d. We assumed that in-channel transversal head variations are negligible because of limited lateral exchange and head varies mostly longitudinally along the streambed. Consequently, hyporheic exchange chiefly varies longitudinally such that we can simplify the hyporheic flow as a 2D problem, considering just the vertical and longitudinal directions. We assumed a homogenous and isotropic hydraulic conductivity and steady-state conditions, such that the governing equation of the hyporheic flow is the Laplace equation:

$$\nabla^2 h_T = 0 \tag{A1.1}$$

where h_T is the energy head. To solve this equation, we set the bottom boundary as impervious at a depth z_d and the upstream and downstream boundary as an energy drop equal to the streambed slope. The water–sediment boundary was set along the mean streambed elevation and equal to the near-bed total head distribution h_T. The following system of equations summarizes these boundary conditions:

$$\begin{cases} h(0,z) = h(\max(x), z) \\ h_T(x,0) = h_s(x,0) + h_L(x,0) + h_{slope}(x) \\ \left.\dfrac{\partial h}{\partial z}\right|_{z=-z_d} = 0 \end{cases} \tag{A1.2}$$

The total energy is the sum of: (a) the energy head induced by small-scale topography, h_s, i.e. boulders and/or pebble clusters, which are modeled as dune-like head loses, (b) large-scale topography, h_L, which is modeled as water surface elevation variations, and (c) the streambed mean slope h_{slope} calculated at the reach scale.

A.1.1. Head variation induced by small scale topography

The near-bed head variations due to small scale topography are modeled as dynamic head losses due to dune-like bed forms following the model of Stonedahl et al. (2010). They propose the following equation for the amplitude of head distributions, h_m

$$h_m = 0.28\frac{V^2}{2g\sqrt{2}\sigma_b}\begin{cases} \left(\frac{2\sqrt{2}\sigma_b}{0.34Y_0}\right)^{3/8} & \text{if } \frac{2\sqrt{2}\sigma_b}{Y_0} \leqslant 0.34 \\ \left(\frac{2\sqrt{2}\sigma_b}{0.34Y_0}\right)^{3/2} & \text{if } \frac{2\sqrt{2}\sigma_b}{Y_0} > 0.34 \end{cases} \tag{A1.3}$$

where g is the gravitational acceleration, V is the mean stream velocity, Y_0 is the mean flow depth, and $2^{3/2}\sigma_b$ is the mean amplitude of the small-scale topography, with σ_b the standard deviation of the small-scale topography variations. The 1D hydraulic model of the surface flow provides the local values of V and Y_0 for the 6 discharges at each cross-section with cross-section spacing every channel width, which is 30 m. The head distributions induced by the small-scale topography at the streambed interface are then represented in terms of a Fourier series of the bed amplitude oscillations modulated by h_m:

$$h_S(x,0) = h_m\sum_{i=1}^{N} a_{S,i}\sin\left(\frac{2\pi i}{L}x - \varphi_{S,i}\right) \tag{A1.4}$$

where $a_{S,i}$ and $\varphi_{S,i}$ are the amplitudes and the phases of the topography data of Fourier harmonics, respectively. N is the number of harmonics considered in the expansion along the longitudinal direction, L is the reach length and x is the longitudinal direction. The number of harmonics considered in the expansion along the longitudinal direction is set to be one less than half of the number of data points to comply with the Nyquist frequency cutoff.

A.1.2. Head variations induced by large scale topography

The near-bed head distribution induced by large-scale topography was modeled in terms of the Fourier series of the water surface elevation:

$$h_L(x,0) = \sum_{i=1}^{M} a_{L,i}\sin\left(\frac{2\pi i}{L}x - \varphi_{L,i}\right) \tag{A1.5}$$

where $a_{L,i}$ and $\varphi_{L,i}$ are the amplitudes and the phases of the water surface elevation of Fourier harmonicas, respectively, and M is the number of harmonics considered in the expansion along the longitudinal direction.

Because the Laplace equation is linear, we can superpose the contribution of each factor independently:

$$h_T(x,0) = h_S(x,0) + h_L(x,0) + h_{slope}(x) \tag{A1.6}$$

where h_{slope} is the head distribution due to the mean streambed slope (s_0).

The solution for Eq. (A1.1) with the boundary and initial conditions expressed by Eqs. (A1.2), (A1.3) and (A1.6) is:

$$\begin{aligned} h(x,z) = {} & h_m\sum_{i=1}^{N} a_{S,i}\sin\left(\frac{2\pi i}{L_S}x - \varphi_{S,i}\right)\left[\tanh\left(\frac{2\pi i}{L}z_d\right)\sinh\left(\frac{2\pi i}{L}z\right)\right. \\ & \left. + \cosh\left(\frac{2\pi i}{L}z\right)\right] + \sum_{i=1}^{M} a_{L,i}\sin\left(\frac{2\pi i}{L}x - \varphi_{L,i}\right) \\ & \times\left[\tanh\left(\frac{2\pi i}{L}z_d\right)\sinh\left(\frac{2\pi i}{L}z\right) + \cosh\left(\frac{2\pi i}{L}z\right)\right] + xs_0 \end{aligned} \tag{A1.7}$$

Once the pressure distribution is known within the hyporheic zone, we compute the velocity field with Darcy's equation (Eq (A1.8)), which relates velocity with the gradient of the pressure head:

$$u(u,w) = -\frac{K}{\phi}\frac{\partial h}{\partial x}, \quad -\frac{K}{\phi}\frac{\partial h}{\partial z} \tag{A1.8}$$

where ϕ is the sediment porosity, which we set equal to 0.34. Because of the coarse material and low percent of fine grains, we set the hydraulic conductivity, $K = 0.005$ m/s.

Once the flow field is known, the hyporheic residence time and the mean upwelling fluxes are predicted with the particle tracking technique (Tonina and Bellin, 2007). The mean upwelling flux for each stream reach is calculated with the following integral:

$$\bar{q}_{uw} = \frac{1}{A_{uw}}\int_A u_{uw}\phi dA_{uw} \tag{A1.9}$$

The equation was applied to calculate the weighted means of the fluxes for each reach.

A.2. Heat transport model

We assumed that the stream water temperature is well-mixed, spatially constant over one morphological unit (e.g. bed feature), and varies temporally following daily temperature oscillations (Marzadri et al., 2012a, 2013a,b). No lateral or bottom heat exchange is specified in the model because of the presence of bedrock. The streambed material was considered to be in local thermal equilibrium. The assumption of local thermal equilibrium implies that at each point the sediment and water temperatures are similar and the effective volumetric heat capacity of the sediment, C, and effective thermal conductivity, K_T, characterize the composite medium of sediment and water (Cardenas and Wilson, 2007b). Under these assumptions, the transport equation for advection, conduction, and dispersion is:

$$C\frac{\partial T}{\partial t} = \frac{\partial}{\partial x_i}\left(K_T\frac{\partial T}{\partial x_i}\right) + \frac{\partial}{\partial x_i}\left(\phi C_w D_{ik}\frac{\partial T}{\partial x_k}\right) - C_w\phi u_i\frac{\partial T}{\partial x_i} \tag{A2.1}$$

where T is the temperature, C_w is the volumetric heat capacity of water, x_i ($i = 1, 2, 3$) are Cartesian coordinates, D_{ik} is the mechanical dispersion coefficient tensor, and u_i ($i = 1, 2, 3$) are the components of the hyporheic flow velocity u. D_{ik} depends mainly on the longitudinal component α_L of the dispersivity because the transversal is typically an order of magnitude smaller (thus $\alpha_T = 0$ and $D_{ik} = \alpha_L u$). Eq. (A2.1) can be written in a more convenient way for the following analytical treatment by applying mass conservation along a stream tube (Bellin and Rubin, 2004; Gelhar and Collins, 1971). The advective, convective and dispersive terms are represented by means of a travel time, τ:

$$\tau = \int_0^l u(\xi)^{-1} d\xi \tag{A2.2}$$

where the integration is performed for any particle along its streamline of length l. Moreover, heat conduction, which stems from the velocity gradient along the trajectories and which is important only deep in the sediment (Cardenas and Wilson, 2007b) is considered to be negligible because velocity gradients are small within the alluvium except near the streambed (Marzadri et al., 2012a). Thus, the heat transport equation along any streamline simplifies to:

$$\frac{\partial T}{\partial t} = D\frac{\partial^2 T}{\partial \tau^2} - C_T\frac{\partial T}{\partial \tau} \tag{A2.3}$$

where

$$D = \frac{\phi \alpha_L C_w}{C|u|} + \frac{K_T}{C|u|^2}; \quad C_T = \phi\frac{C}{C_w} \tag{A2.4}$$

We assume the groundwater temperature (T_{GW}) as an initial condition within the sediment $T(\tau,0)$ for Eq. (A2.3), that downwelling fluxes have stream temperature $T_s(t)$ and that temperature gradients are negligible at the upwelling end of any streamline:

$$\begin{cases} T(\tau,0) = T_{GW}(\tau,0); \\ T(0,t) = T_s(t); \\ \left.\dfrac{\partial T}{\partial \tau}\right|_{\tau\to\infty} = 0 \end{cases} \tag{A2.5}$$

The in-stream temperature daily variations can be represented in terms of the Fourier series as a superposition of a constant mean (T_0) and a periodic fluctuation:

$$T_s(t) = T_0 + 2\sum_{i=1}^{NT} T_{A,i1}\sin(\omega_i t) + 2\sum_{i=1}^{NT} T_{A,i2}\cos(\omega_i t) \tag{A2.6}$$

with

$$\begin{cases} T_0 = a_{T,0}\sin(-\varphi_{T,0}); \\ T_{A,i1} = a_{T,i}\cos(-\varphi_{T,i}); \\ T_{A,i2} = a_{T,i}\sin(-\varphi_{T,i}) \end{cases} \tag{A2.7}$$

where $a_{T,i}$ and $\varphi_{T,i}$ ($i = 0\ldots$NT) are the amplitude and the phase of the temperature data of the NT Fourier harmonics, respectively.

Following the approach proposed by Alshawabkeh and Adrian (1997) and considering that along the Lower Deadwood River the pertinent temperature oscillations were at the same period of fluctuation of the in-stream water (1 day), the simplified solution of Eq. (A2.3) (Marzadri et al., 2013a,b) with initial and boundary conditions of Eqs. (A2.6) and (A2.7), is:

$$\begin{aligned} T(\tau,t) = {} & \frac{T_0 - T_{GW}}{2}\left[\exp\left(\frac{C_T}{D}\tau\right) erfc\left(\frac{\tau + C_T t}{2\sqrt{Dt}}\right) + erfc\left(\frac{\tau - C_T t}{2\sqrt{Dt}}\right)\right] \\ & + \sum_{i=1}^{NT} T_{A,i1}\exp\left(\frac{C_T\tau}{2D} - a_i\right)\sin(\omega_i t - b_i) - \sum_{i=1}^{NT} T_{A,i2} \\ & \times \exp\left(\frac{C_T\tau}{2D} - a_i\right)\cos(\omega_i t - b_i) + T_{GW} \end{aligned} \tag{A2.8}$$

This simplified solution was used for predicting the hyporheic water temperature at the probe locations at the study site (Reach 15). The analysis showed that the first six harmonics suffice to represent the temperature fluctuations with the Fourier series; therefore in the simulations NT = 5. On the other hand, for analyzing the effects of small and large scales on the hyporheic thermal response along the whole course of the Lower Deadwood River, it was assumed that in any reach $T_s(t)$ can be represented as the sum of a constant component T_0 and a dial sinusoidal component given by the following equation:

$$T_S(t) = T_0 + T_A\sin\left(\frac{2\pi}{t_d}t\right) \tag{A2.9}$$

where T_A is the daily temperature amplitude, and t_d is the fluctuation period (1 day). In this case, the solution of Eq. (A2.3), with the other two boundary conditions (A2.4) remaining unaltered, is:

$$\begin{aligned} T_A(\tau,t) = {} & \frac{T_0 - T_{GW}}{2}\left[\exp\left(\frac{C_T}{D}\tau\right) erfc\left(\frac{\tau + C_T t}{2\sqrt{Dt}}\right) + erfc\left(\frac{\tau - C_T t}{2\sqrt{Dt}}\right)\right] \\ & + T_{GW} + T_A\exp\left(\frac{C_T}{D}\tau - a\right)\sin(\omega t - b) \end{aligned} \tag{A2.10}$$

References

Allan, J.D., 1995. Stream Ecology Structure and Function of Running Waters. Chapman and Hall, London, UK.

Alshawabkeh, A., Adrian, D.D., 1997. Analytical water quality model for a sinusoidally varying BOD discharge concentration. Water Resour. Res. 31 (5), 1207–1215.

Barnes, H.H.J., 1967. Roughness Characteristics of Natural Channels. United States Government Printing Office, Washington, DC, 213pp.

Bellin, A., Rubin, Y., 2004. On the use of peak concentration arrival times for influence of hydrogeological parameters. Water Resour Res 40, 1–10.

Bencala, K.E., Walters, R.A., 1983. Simulation of solute transport in a mountain pool-and-riffle stream: a transient storage model. Water Resour. Res. 19 (3), 718–724.

Benjankar, R.M., Tranmer, A., Tiedemann, M.G., Tonina, D., 2013. Analysis of an impact of different discharge scenarios on the thermal regime of the stream below the Dead Wood Reservoir in the central Idaho, USA, 35th IAHR World Congress 2013. Tsinghua University Press, Chengdu, China.

Benjankar, R., Tonina, D., McKean, J.A., 2014. One-dimensional and two-dimensional hydrodynamic modeling derived flow properties: impacts on aquatic habitat quality predictions. Earth Surf. Proc. Land. http://dx.doi.org/10.1002/esp.3637.

Bjornn, T.C., Reiser, D.W., 1991. Habitat requirements of salmonids in streams. In: Meehan, W.R. (Ed.), Influence of Forest and Rangeland Management on Salmonid Fishes and Their Habitats. Am. Fish. Soc. Spec. Publ. 19. Bethesda, Md., pp. 83–138.

Boano, F., Revelli, R., Ridolfi, L., 2007. Bedform-induced hyporheic exchange with unsteady flows. Adv. Water Resour. 30, 148–156.

Boano, F., Poggi, D., Revelli, R., Ridolfi, L., 2009. Gravity-driven water exchange between streams and hyporheic zones. Geophys. Res. Lett. 36, L20402. http://dx.doi.org/10.1029/2009GL040147.

Boano, F., Demaria, A., Revelli, R., Ridolfi, L., 2010. Biogeochemical zonation due to intrameander hyporheic flow. Water Resour. Res. 46, W02511. http://dx.doi.org/10.1029/2008WR007583.

Boano, F., Harvey, J.W., Marion, A., Packman, A.I., Revelli, R., Ridolfi, L., Wörman, A., 2014. Hyporheic flow and transport processes: mechanisms, models, and biogeochemical implications. Rev. Geophys. http://dx.doi.org/10.1002/2012RG000417.

Bruno, M.C., Maiolini, B., Carolli, M., Silveri, L., 2009. Impact of hydropeaking on hyporheic invertebrates in an Alpine stream (Trentino, Italy). Int. J. Limnol. 45, 157–170.

Buffington, J.M., Tonina, D., 2009. Hyporheic exchange in mountain rivers II: effects of channel morphology on mechanics, scales, and rates of exchange. Geogr. Compass 3 (3), 1038–1062.

Cardenas, M.B., 2009. Stream-aquifer interactions and hyporheic exchange in gaining and losing sinuous streams. Water Resour. Res. 45, W06429. http://dx.doi.org/10.1029/2008WR007651.

Cardenas, B.M., Wilson, J.L., 2007a. Dune, turbulent eddies, and interfacial exchange with permeable sediments. Water Resour. Res. 43, W08412. http://dx.doi.org/10.1029/2006WR005787.

Cardenas, M.B., Wilson, J.L., 2007b. Effects of current-bed form induced fluid flow on thermal regime of sediments. Water Resour. Res. 43, W08431. http://dx.doi.org/10.1029/2006WR005343.

Cardenas, M.B., Wilson, J.L., 2007c. Exchange across a sediment–water interface with ambient groundwater discharge. J. Hydrol. 346, 69–80. http://dx.doi.org/10.1016/j.jhydrol.2007.08.019.

Cardenas, M.B., Wilson, J.L., 2007d. Hydrodynamics of coupled flow above and below a sediment–water interface with triangular bedforms. Adv. Water Resour. 30, 301–313.

Cardenas, M.B., Wilson, J.F., Zlotnik, V.A., 2004. Impact of heterogeneity, bed forms, and stream curvature on subchannel hyporheic exchange. Water Resour. Res. 40 (W08307). http://dx.doi.org/10.1029/2004WR003008.

Edwards, R.T., 1998. The Hyporheic Zone. In: Naiman, R.J., Bilby, R.E. (Eds.), River Ecology and Management: Lessons from the Pacific Coastal Ecoregion. Springer-Verlag, New York, pp. 399–429.

Elliott, A., Brooks, N.H., 1997a. Transfer of nonsorbing solutes to a streambed with bed forms: laboratory experiments. Water Resour. Res. 33 (1), 137–151.

Elliott, A., Brooks, N.H., 1997b. Transfer of nonsorbing solutes to a streambed with bed forms: theory. Water Resour. Res. 33 (1), 123–136.

Fox, A., Boano, F., Amon, S., 2014. Impact of losing and gaining streamflow conditions on hyporheic exchange fluxes induced by dune-shaped bed forms. Water Resour. Res. 50, 1895–1907. http://dx.doi.org/10.1002/2013WR014668.

Gariglio, F., Tonina, D., Luce, C.H., 2013. Spatio-temporal variability of hyporheic exchange through a pool–riffle–pool sequence. Water Resour. Res. 49 (11), 7185–7204. http://dx.doi.org/10.1002/wrcr.20419.

Gelhar, L.W., Collins, M.A., 1971. General analysis of longitudinal dispersion in nonuniform flow. Water Resour. Res. 7 (6), 1511–1521.

Goode, J.R., Buffington, J.M., Tonina, D., Isaak, D.J., Thurow, R.F., Wenger, S., Nagel, D., Luce, C.H., Tetzlaff, D., Soulsby, C., 2013. Potential effects of climate change on streambed scour and risks to salmonid survival in snow-dominated mountain basins. Hydrol. Process. 27, 750–765. http://dx.doi.org/10.1002/hyp.9728.

Gooseff, M.N., Anderson, J.K., Wondzell, S.M., LaNier, J., Haggerty, R., 2006. A modelling study of hyporheic exchange pattern and the sequence, size, and spacing of stream bedforms in mountain stream networks, Oregon, USA. Hydrol. Process. 20 (11), 2443–2457.

Gooseff, M.N., Hall, R.O.J., Tank, J.L., 2007. Relating transient storage to channel complexity in streams of varying land use in Jackson Hole, Wyoming. Water Resour. Res. 43 (W01417). http://dx.doi.org/10.1029/2005WR004626.

Gualtieri, C., 2012. Effect of Permeability on Hyporheic Flows Across a Triangular Dune. In: Dragutin, T.M. (Ed.), Essays on Fundamental and Applied Environmental Topics. Nova Science, New York, USA.

Harvey, J.W., Böhlke, J.K., Voytek, M.A., Scott, D., Tobias, C.R., 2013. Hyporheic zone denitrification: controls on effective reaction depth and contribution to whole-stream mass balance. Water Resour. Res. 49 (10). http://dx.doi.org/10.1002/wrcr.20492.

Hester, E.T., Young, K.I., Widdowson, M.A., 2013. Mixing of surface and groundwater induced by riverbed dunes: implications for hyporheic zone definitions and pollutant reactions. Water Resour. Res. 49, 5221–5237.

Jonsson, K., Johansson, H., Wörman, A., 2004. Sorption behavior and long-term retention of reactive solutes in the hyporheic zone of streams. J. Environ. Eng. 130 (5). http://dx.doi.org/10.1061/(ASCE)0733-9372(2004) 130:5(573.

Kasahara, T., Hill, A.R., 2006a. Effects of riffle–step restoration on hyporheic zone chemistry in N-rich lowland streams. Can. J. Fish. Aquat. Sci. 63, 120–133. http://dx.doi.org/10.1139/F05-199.

Kasahara, T., Hill, A.R., 2006b. Hyporheic exchange flows induced by constructed riffles and steps in lowland streams in southern Ontario, Canada. Hydrol. Process. 20, 4287–4305. http://dx.doi.org/10.1002/hyp.6174.

Kasahara, T., Hill, A.R., 2007. Lateral hyporheic zone chemistry in an artificially constructed gravel bar and a re-meandered stream channel, Southern Ontario, Canada. J. Am. Water Resour. Assoc. 43 (5).

Kasahara, T., Datry, T., Mutz, M., Boulton, A.J., 2009. Treating causes not symptoms: restoration of surface–groundwater interactions in rivers. Mar. Freshw. Res. 60, 976–981.

Kennedy, C.D., Genereux, D.P., Corbett, D.R., Mitasova, H., 2009. Spatial and temporal dynamics of coupled groundwater and nitrogen fluxes through a streambed in an agricultural watershed. Water Resour. Res. 45, W09401. http://dx.doi.org/10.1029/2008WR007397.

Lautz, L., Siegel, D.I., 2006. Modeling surface and ground water mixing in the hyporheic zone using MODFLOW and MT3D. Adv. Water Resour. 29 (11), 1618–1633. http://dx.doi.org/10.1016/j.advwatres.2005.12.003.

Leopold, L.B., Wolman, M.G., 1957. River Channel Patterns: Braided, Meandering, and Straight. U.S. Geological Survey, pp. 39–84.

Marion, A., Bellinello, M., Guymer, I., Packman, A.I., 2002. Effect of bed form geometry on the penetration of nonreactive solutes into a streambed. Water Resour. Res. 38 (10), 1209. http://dx.doi.org/10.1029/2001WR000264.

Marion, A., Packman, A.I., Zaramella, M., Bottacin-Busolin, A., 2008a. Hyporheic flows in stratified beds. Water Resour. Res. 44, W09433. http://dx.doi.org/10.1029/2007WR006079.

Marion, A., Zaramella, M., Bottacin-Busolin, A., 2008b. Solute transport in rivers with multiple storage zones: the STIR model. Water Resour. Res. 44, W10406. http://dx.doi.org/10.1029/2008WR007037.

Marzadri, A., Tonina, D., Bellin, A., Vignoli, G., Tubino, M., 2010. Effects of bar topography on hyporheic flow in gravel-bed rivers. Water Resour. Res. 46, W07531. http://dx.doi.org/10.1029/2009WR008285.

Marzadri, A., Tonina, D., Bellin, A., 2011. A semianalytical three-dimensional process-based model for hyporheic nitrogen dynamics in gravel bed rivers. Water Resour. Res. 47, W11518. http://dx.doi.org/10.1029/2011WR010583.

Marzadri, A., Tonina, D., Bellin, A., 2012a. Effects of hyporheic fluxes on streambed pore water temperature. In: 10th International Conference on Hydroinformatics HIC 2012. IAHR, Hamburg, Germany.

Marzadri, A., Tonina, D., Bellin, A., 2012b. Morphodynamic controls on redox conditions and on nitrogen dynamics within the hyporheic zone: application to gravel bed rivers with alternate-bar morphology. J. Geophys. Res. 117. http://dx.doi.org/10.1029/2012JG001966.

Marzadri, A., Tonina, D., Bellin, A., 2013a. Effects of stream morphodynamics on hyporheic zone thermal regime. Water Resour. Res. 49 (4), 2287–2302. http://dx.doi.org/10.1002/wrcr.20199.

Marzadri, A., Tonina, D., Bellin, A., 2013b. Quantifying the importance of daily stream water temperature fluctuations on the hyporheic thermal regime: Implication for dissolved oxygen dynamics. J. Hydrol. 507, 241–248. http://dx.doi.org/10.1016/j.jhydrol.2013.10.030.

Marzadri, A., Tonina, D., Bellin, A., Tank, J.L., 2014. A hydrologic model demonstrates nitrous oxide emissions depend on streambed morphology. Geophys. Res. Lett. 41 (15), 5484–5491. http://dx.doi.org/10.1002/2014GL060732.

McKean, J.A., Nagel, D., Tonina, D., Bailey, P., Wright, C.W., Bohn, C., Nayegandhi, A., 2009. Remote sensing of channels and riparian zones with a narrow-beam aquatic-terrestrial LIDAR. Remote Sens. 1, 1065–1096. http://dx.doi.org/10.3390/rs1041065.

McKean, J.A., Tonina, D., Bohn, C., Wright, C.W., 2014. Effects of bathymetric lidar errors on flow properties predicted with a multi-dimensional hydraulic model. J. Geophys. Res.: Earth Surf. http://dx.doi.org/10.1002/2013JF002897.

Montgomery, D.R., Buffington, J.M., 1998. Channel Processes, Classification, and Response. In: Naiman, R., Bilby, R. (Eds.), River Ecology and Management. Springer-Verlag, NY, pp. 13–42.

Niswonger, R.G., Prudic, D.E., Pohll, G., Constantz, J., 2005. Incorporating seepage losses into the unsteady streamflow equations for simulating intermittent flow along mountain front streams. Water Resour. Res. 41, W06006. http://dx.doi.org/10.1029/2004WR003677.

Packman, A.I., Salehin, M., Zaramella, M., 2004. Hyporheic exchange with gravel beds: basic hydrodynamic interactions and bedform-induced advective flows. J. Hydraul. Eng. 130 (7), 647–656, doi: 10.1061/(ASCE)0733-9429(2004)130:7(647).

Parkinson, S.K., 2003. Project Hydrology and Hydraulic Models Applied to the Hells Canyon Reach of the Snake River Hells Canyon Complex FERC No. 1971. Idaho Power Company, Boise, ID.

Pasternack, G.B., Senter, A., 2011. 21st Century Instream Flow Assessment Framework for Mountain Streams, Public Interest Energy Research (PIER), California Energy Commission.

Rau, G.C., Andersen, M.S., Acworth, R.I., 2012. Experimental investigation of the thermal dispersivity term and its significance in the heat transport equation for flow in sediments. Water Resour. Res. 48, W03511. http://dx.doi.org/10.1029/2011WR011038.

Rosgen, D.L., 1994. A classification of natural rivers. Catena 22, 169–199.

Rosgen, D.L., 1996. Applied River Morphology. Wildland Hydrology, Pagosa Springs, Colorado.

Salehin, M., Packman, A.I., Paradis, M., 2004. Hyporheic exchange with heterogeneous streambeds: laboratory experiments and modeling. Water Resour. Res. 40 (11). http://dx.doi.org/10.1029/2003WR002567.

Savant, A.S., Reible, D.D., Thibodeaux, L.J., 1987. Convective transport within stable river sediments. Water Resour. Res. 23 (9), 1763–1768.

Sawyer, A.H., Cardenas, B.M., Bomar, A., Macley, M., 2009. Impact of dam operations on hyporheic exchange in the riparian zone of a regulated river. Hydrol. Process. 23, 2129–2137. http://dx.doi.org/10.1002/hyp.7324.

Sawyer, A.H., Cardenas, B.M., Buttles, J., 2011. Hyporheic exchange due to channel-spanning logs. Water Resour. Res. 47, W08502. http://dx.doi.org/10.1029/2010WR010484.

Sawyer, A.H., Cardenas, B.M., Buttles, J., 2012. Hyporheic temperature dynamics and heat exchange near channel-spanning logs. Water Resour. Res. 48, W01529. http://dx.doi.org/10.1029/2011WR011200.

Stanford, J.A., Ward, J.V., 1988. The hyporheic habitat of river ecosystems. Nature 335, 64–65.

Stewart, R.J., Wollheim, W.M., Gooseff, M.N., Briggs, M.A., Jacobs, J.M., Peterson, B.J., Hopkinson, C.S., 2011. Separation of river network-scale nitrogen removal among the main channel and two transient storage compartments. Water Resour. Res. 47, W00J10. http://dx.doi.org/10.1029/2010WR009896.

Stonedahl, S.H., Harvey, J.W., Wörman, A., Salehin, M., Packman, A.I., 2010. A multi-scale model for integrating hyporheic exchange from ripples to meanders. Water Resour. Res. 46, W12539. http://dx.doi.org/10.1029/2009WR008865.

Stonedahl, S.H., Harvey, J.W., Detty, J., Aubeneau, A., Packman, A.I., 2012. Physical controls and predictability of stream hyporheic flow evaluated with a multiscale model. Water Resour. Res. 48, W10513. http://dx.doi.org/10.1029/2011WR011582.

Stonedahl, S.H., Harvey, J.W., Packman, A.I., 2013. Interactions between hyporheic flow produced by stream meanders, bars, and dunes. Water Resour. Res. 49, 5450–5461. http://dx.doi.org/10.1002/wrcr.20400.

Thibodeaux, L.J., Boyle, J.D., 1987. Bedform-generated convective transport in bottom sediment. Nature 325 (22), 341–343.

Tiedemann, M.G., 2013. Examining a Functional Flow Regime and Accompanying Thermal Regime in a Regulated Mountain Canyon River under Varying Climatic Conditions. University of Idaho, Boise, Idaho, 84pp.

Tonina, D., 2012. Surface Water and Streambed Sediment Interaction: The Hyporheic Exchange. In: Gualtieri, C., Mihailović, D.T. (Eds.), Fluid Mechanics of Environmental Interfaces. CRC Press, Taylor & Francis Group, London, UK, pp. 255–294.

Tonina, D., Bellin, A., 2007. Effects of pore-scale dispersion, degree of heterogeneity, sampling size, and source volume on the concentration moments of conservative solutes in heterogeneous formations. Adv. Water Resour. http://dx.doi.org/10.1016/j.advwatres.2007.08.009.

Tonina, D., Buffington, J.M., 2007. Hyporheic exchange in gravel-bed rivers with pool–riffle morphology: laboratory experiments and three-dimensional modeling. Water Resour. Res. 43 (W01421).

Tonina, D., Buffington, J.M., 2009a. Hyporheic exchange in mountain rivers I: Mechanics and environmental effects Geography. Compass 3 (3), 1063–1086.

Tonina, D., Buffington, J.M., 2009b. A three-dimensional model for analyzing the effects of salmon redds on hyporheic exchange and egg pocket habitat. Can. J. Fish. Aquat. Sci. 66, 2157–2173. http://dx.doi.org/10.1139/F09-146.

Tonina, D., Buffington, J.M., 2011. Effects of stream discharge, alluvial depth and bar amplitude on hyporheic flow in pool–riffle channels. Water Resour. Res. 47, W08508. http://dx.doi.org/10.1029/2010WR009140.

Tonina, D., Jorde, K., 2013. Hydraulic Modeling Approaches for Ecohydraulic Studies: 3D, 2D, 1D and non-Numerical Models. In: Maddock, I., Wood, P.J., Harby, A., Kemp, P. (Eds.), Ecohydraulics: An Integrated Approach. Wiley-Blackwell, New Delhi, India, pp. 31–66.

Tonina, D., Marzadri, A., Bellin, A., 2011. Effect of hyporheic flows induced by alternate bars on benthic oxygen uptake. 34th IAHR World Congress 2011. IAHR, Brisbane, Australia, pp. 3129–3136.

Tonina, D., Luce, C.H., Gariglio, F., 2014. Quantifying streambed deposition and scour from stream and hyporheic water temperature time series. Water Resour. Res. 50 (1), 1–6. http://dx.doi.org/10.1002/2013WR014567.

Tranmer, A., Tonina, D., Goodwin, P., Benjankar, R.M., Tiedemann, M.G., 2013. Stream power changes in an alluvial canyon – Deadwood River, USA. 35th IAHR World Congress 2013. Tsinghua University Press, Chengdu, China.

Trauth, N., Schimdt, C., Maier, U., Vieweg, M., Fleckenstein, J.H., 2013. Coupled 3D stream flow and hyporheic flow model under varying stream and ambient groundwater flow conditions in pool–riffle system. Water Resour. Res. 49 (9). http://dx.doi.org/10.1002/wrcr.20442.

Vaux, W.G., 1962. Interchange of stream and intragravel water in a salmon spawning riffle. Fisheries No 405. US Fish and Wildlife Service. Bureau of Commercial Fisheries, Washington, DC.

Vaux, W.G., 1968. Intragravel flow and interchange of water in a streambed. Fish. Bull. 66 (3), 479–489.

Vittal, N., Ranga Raju, K.G., Garde, R.J., 1977. Resistance of two-dimensional triangular roughness. J. Hydraul. Res. 15 (1), 19–36.

Woessner, W.W., 2000. Stream and fluvial plain ground water interactions: rescaling hydrogeologic thought. Ground Water 38 (3), 423–429.

Wondzell, S.M., 2011. The role of the hyporheic zone across stream networks. Hydrol. Process. 25 (22), 3525–3532.

Wörman, A., Packman, A.I., Johansson, H., Jonsson, K., 2002. Effect of flow-induced exchange in hyporheic zones on longitudinal transport of solutes in streams and rivers. Water Resour. Res. 38 (1), 15. http://dx.doi.org/10.1029/2001WR000769.

Wörman, A., Packman, A.I., Marklund, L., Harvey, J.W., 2006. Exact three-dimensional spectral solution to surface-groundwater interaction with arbitrary surface topography. Geophys. Res. Lett. 33 (L07402). http://dx.doi.org/10.1029/2006GL025747.

Zarnetske, J.P., Gooseff, M.N., Bowden, B.W.G., Morgan, J., Brosten, T.R., Bradford, J.H., McNamara, J.P., 2008. Influence of morphology and permafrost dynamics on hyporheic exchange in arctic headwater streams under warming climate conditions. Geophys. Res. Lett. 35 (L02501). http://dx.doi.org/10.1029/2007GL032049.

Zarnetske, J.P., Haggerty, R., Wondzell, S.M., Baker, M.A., 2011. Dynamics of nitrate production and removal as a function of residence time in the hyporheic zone. J. Geophys. Res. 116, G01025. http://dx.doi.org/10.1029/2010JG001356.

Zarnetske, J.P., Haggerty, R., Wondzell, S.M., Bokil, V.A., González-Pinzón, R., 2012. Coupled transport and reaction kinetics control the nitrate source-sink function of hyporheic zones. Water Resour. Res. 48, W11508. http://dx.doi.org/10.1029/2012WR011894.

Zijl, W., 1999. Scale aspects of groundwater flow and transport system. Hydrogeol. J. 7, 139–150.